

# Study of the doubly and singly Cabibbo suppressed decays $D^+ \rightarrow K^+\pi^+\pi^-$ and $D_s^+ \rightarrow K^+\pi^+\pi^-$

The FOCUS Collaboration

J. M. Link<sup>a</sup> P. M. Yager<sup>a</sup> J. C. Anjos<sup>b</sup> I. Bediaga<sup>b</sup> C. Göbel<sup>b</sup>  
 A. A. Machado<sup>b</sup> J. Magnin<sup>b</sup> A. Massafferri<sup>b</sup>  
 J. M. de Miranda<sup>b</sup> I. M. Pepe<sup>b</sup> E. Polcarpo<sup>b</sup> A. C. dos Reis<sup>b</sup>  
 S. Carrillo<sup>c</sup> E. Casimiro<sup>c</sup> E. Cuautle<sup>c</sup> A. Sánchez-Hernández<sup>c</sup>  
 C. Uribe<sup>c</sup> F. Vázquez<sup>c</sup> L. Agostino<sup>d</sup> L. Cinquini<sup>d</sup>  
 J. P. Cumalat<sup>d</sup> B. O'Reilly<sup>d</sup> I. Segoni<sup>d</sup> K. Stenson<sup>d</sup>  
 J. N. Butler<sup>e</sup> H. W. K. Cheung<sup>e</sup> G. Chiodini<sup>e</sup> I. Gaines<sup>e</sup>  
 P. H. Garbincius<sup>e</sup> L. A. Garren<sup>e</sup> E. Gottschalk<sup>e</sup> P. H. Kasper<sup>e</sup>  
 A. E. Kreymer<sup>e</sup> R. Kutschke<sup>e</sup> M. Wang<sup>e</sup> L. Benussi<sup>f</sup>  
 M. Bertani<sup>f</sup> S. Bianco<sup>f</sup> F. L. Fabbri<sup>f</sup> A. Zallo<sup>f</sup> M. Reyes<sup>g</sup>  
 C. Cawfield<sup>h</sup> D. Y. Kim<sup>h</sup> A. Rahimi<sup>h</sup> J. Wiss<sup>h</sup> R. Gardner<sup>i</sup>  
 A. Kryemadhi<sup>i</sup> Y. S. Chung<sup>j</sup> J. S. Kang<sup>j</sup> B. R. Ko<sup>j</sup>  
 J. W. Kwak<sup>j</sup> K. B. Lee<sup>j</sup> K. Cho<sup>k</sup> H. Park<sup>k</sup> G. Alimonti<sup>ℓ</sup>  
 S. Barberis<sup>ℓ</sup> M. Boschini<sup>ℓ</sup> A. Cerutti<sup>ℓ</sup> P. D'Angelo<sup>ℓ</sup>  
 M. DiCorato<sup>ℓ</sup> P. Dini<sup>ℓ</sup> L. Edera<sup>ℓ</sup> S. Erba<sup>ℓ</sup> M. Giammarchi<sup>ℓ</sup>  
 P. Inzani<sup>ℓ</sup> F. Leveraro<sup>ℓ</sup> S. Malvezzi<sup>ℓ</sup> D. Menasce<sup>ℓ</sup>  
 M. Mezzadri<sup>ℓ</sup> L. Moroni<sup>ℓ</sup> D. Pedrini<sup>ℓ</sup> C. Pontoglio<sup>ℓ</sup> F. Prelz<sup>ℓ</sup>  
 M. Rovere<sup>ℓ</sup> S. Sala<sup>ℓ</sup> T. F. Davenport III<sup>m</sup> V. Arena<sup>n</sup> G. Boca<sup>n</sup>  
 G. Bonomi<sup>n</sup> G. Gianini<sup>n</sup> G. Liguori<sup>n</sup> M. M. Merlo<sup>n</sup>  
 D. Pantea<sup>n</sup> D. Lopes Pegna<sup>n</sup> S. P. Ratti<sup>n</sup> C. Riccardi<sup>n</sup>  
 P. Vitulo<sup>n</sup> H. Hernandez<sup>o</sup> A. M. Lopez<sup>o</sup> H. Mendez<sup>o</sup> A. Paris<sup>o</sup>  
 J. Quinones<sup>o</sup> J. E. Ramirez<sup>o</sup> Y. Zhang<sup>o</sup> J. R. Wilson<sup>p</sup>  
 T. Handler<sup>q</sup> R. Mitchell<sup>q</sup> A. D. Bryant<sup>r</sup> D. Engh<sup>r</sup> M. Hosack<sup>r</sup>  
 W. E. Johns<sup>r</sup> E. Luiggi<sup>r</sup> M. Nehring<sup>r</sup> P. D. Sheldon<sup>r</sup>  
 E. W. Vaandering<sup>r</sup> M. Webster<sup>r</sup> M. Sheaff<sup>s</sup>

<sup>a</sup>*University of California, Davis, CA 95616*

<sup>b</sup>*Centro Brasileiro de Pesquisas Físicas, Rio de Janeiro, RJ, Brasil*

<sup>c</sup>*CINVESTAV, 07000 México City, DF, Mexico*

<sup>d</sup>*University of Colorado, Boulder, CO 80309*

<sup>e</sup>*Fermi National Accelerator Laboratory, Batavia, IL 60510*

<sup>f</sup>*Laboratori Nazionali di Frascati dell'INFN, Frascati, Italy I-00044*

<sup>g</sup>*University of Guanajuato, 37150 Leon, Guanajuato, Mexico*

<sup>h</sup>*University of Illinois, Urbana-Champaign, IL 61801*

<sup>i</sup>*Indiana University, Bloomington, IN 47405*

<sup>j</sup>*Korea University, Seoul, Korea 136-701*

<sup>k</sup>*Kyungpook National University, Taegu, Korea 702-701*

<sup>l</sup>*INFN and University of Milano, Milano, Italy*

<sup>m</sup>*University of North Carolina, Asheville, NC 28804*

<sup>n</sup>*Dipartimento di Fisica Nucleare e Teorica and INFN, Pavia, Italy*

<sup>o</sup>*University of Puerto Rico, Mayaguez, PR 00681*

<sup>p</sup>*University of South Carolina, Columbia, SC 29208*

<sup>q</sup>*University of Tennessee, Knoxville, TN 37996*

<sup>r</sup>*Vanderbilt University, Nashville, TN 37235*

<sup>s</sup>*University of Wisconsin, Madison, WI 53706*

See <http://www-focus.fnal.gov/authors.html> for additional author information.

---

## Abstract

Using data collected by the high energy photoproduction experiment FOCUS at Fermilab we study the doubly and singly Cabibbo suppressed decays  $D^+$  and  $D_s^+ \rightarrow K^+\pi^+\pi^-$ . Our measurements of  $\Gamma(D^+ \rightarrow K^+\pi^+\pi^-)/\Gamma(D^+ \rightarrow K^-\pi^+\pi^+) = 0.0065 \pm 0.0008 \pm 0.0004$  and  $\Gamma(D_s^+ \rightarrow K^+\pi^+\pi^-)/\Gamma(D_s^+ \rightarrow K^+K^-\pi^+) = 0.127 \pm 0.007 \pm 0.014$  are based on samples of  $189 \pm 24$   $D^+$  and  $567 \pm 31$   $D_s^+$  reconstructed events, respectively. We also present Dalitz plot analyses of the two decay channels; the amplitude analysis of the  $D_s^+ \rightarrow K^+\pi^+\pi^-$  mode is performed for the first time.

---

## 1 Introduction

A thorough understanding of  $D$  hadronic decays requires both branching ratio measurements of all the hadronic modes and Dalitz plot analyses to investigate the decay dynamics and probe the role of final state interactions. In this letter we present branching ratio measurements and Dalitz plot analyses of the doubly and singly Cabibbo suppressed decays  $D^+ \rightarrow K^+\pi^+\pi^-$  and  $D_s^+ \rightarrow K^+\pi^+\pi^-$ .

The naïve expectation for the ratio of Doubly Cabibbo Suppressed (DCS)

to Cabibbo Favored (CF) branching fractions is  $\tan^4 \theta_C \sim 0.25\%$ . However the CF  $D^+ \rightarrow K^- \pi^+ \pi^+$  rate could be suppressed by destructive interference between spectator amplitudes with indistinguishable quarks in the final state; this is the argument generally proposed to explain the lifetime difference between  $D^+$  and  $D^0$ . For the hadronic DCS  $D^+$  decay all the final state quarks are different and no destructive interference is present. In this simple picture we would expect, neglecting effects of final state interactions,  $\tau(D^+)/\tau(D^0) = \Gamma(D_{\text{CF}}^0)/\Gamma(D_{\text{CF}}^+) = (1/\tan^4 \theta_C) \times \Gamma(D_{\text{DCS}}^+)/\Gamma(D_{\text{CF}}^+)$ . The comparison of the precise FOCUS lifetime ratio [1]  $\tau(D^+)/\tau(D^0) = 2.538 \pm 0.023$  with the branching ratio  $\Gamma(D_{\text{DCS}}^+)/\Gamma(D_{\text{CF}}^+)$  measurement reported here will test this interpretation.

The final  $D^+$  and  $D_s^+$  samples are selected with cuts to reduce reflections from the more copious Cabibbo favored modes and to optimize the signal to noise ratios, which are crucial for reliable decay amplitude analyses. Dalitz plot analyses have indeed emerged as a unique tool to fully exploit the available charm statistics allowing, besides the simple branching ratio evaluation, to investigate the underlying decay dynamics. Our understanding of the charm decay dynamics has already considerably improved in the last years, but is still limited to a few decay channels. The Dalitz plot analysis of the Singly Cabibbo Suppressed decay (SCS)  $D_s^+ \rightarrow K^+ \pi^+ \pi^-$  is performed for the first time.

## 2 Signal selection

The data for this analysis were collected during the 1996–1997 run of the photoproduction experiment FOCUS at Fermilab. The detector, designed and used to study the interaction of high-energy photons on a segmented BeO target, is a large aperture, fixed-target magnetic spectrometer with excellent Čerenkov particle identification and vertexing capabilities. Most of the FOCUS experiment and analysis techniques have been described previously [2–4].

The suppressed nature of the channels under study requires severe cuts to eliminate reflections, both in the signal and sideband regions, from more copious and favored decays, when one or two charged particles are Čerenkov misidentified and/or one neutral particle is missing. Tight cut choices are also required to improve the signal-to-noise ratio to perform a reliable Dalitz plot analysis.

The  $D^+$  and  $D_s^+$  candidates are obtained using a candidate driven vertex algorithm. A decay vertex is formed from three reconstructed charged tracks. The momentum of the  $D$  candidate is used to intersect other reconstructed tracks to form a production vertex. The confidence levels (C.L.) of each vertex

is required to exceed 1%. From the vertexing algorithm, the variable  $\ell$ , which is the separation of the primary and secondary vertices, and its associated error  $\sigma_\ell$  are calculated. We reduce backgrounds by requiring  $\ell/\sigma_\ell > 14$  and 10 for the  $D^+$  and  $D_s^+$ , respectively. The two vertices are also required to satisfy isolation conditions. The primary vertex isolation cut requires that a track assigned to the decay vertex has a C.L. less than 1% to be included in the primary vertex. The secondary vertex isolation cut requires that all remaining tracks not assigned to the primary and secondary vertex have a C.L. smaller than 0.1% to form a vertex with the  $D$  candidate daughters. The decay vertex is required to be  $3\sigma$  outside of the target material to reduce the background due to hadronic re-interactions in the target.

The Čerenkov particle identification is based on likelihood ratios between the various stable particle hypotheses [3]. The product of all firing probabilities for all cells within the three Čerenkov cones produces a  $\chi^2$ -like variable  $W_i = -2\ln(\text{likelihood})$  where  $i$  ranges over the electron, pion, kaon and proton hypothesis. For the  $D^+$  selection, we require  $\Delta W_K = W_\pi - W_K > 4$  and  $\Delta W_\pi = W_K - W_\pi > 3.5$  for both pions in the final state. For the  $D_s^+$  candidates we require  $\Delta W_K > 4$  for the kaon,  $\Delta W_\pi > 2$  for opposite-sign pion and  $\Delta W_\pi > 1$  for same-sign pion. These selections minimize the contamination from charm background.

A detailed Monte Carlo study is performed to evaluate the possible contaminations and structures induced by reflections both in the signal and sideband regions.<sup>1</sup> The considered sources of background are the  $D^+$  and  $D_s^+$  three-body hadronic decays, where one or two particles are misidentified, and four-body hadronic and semileptonic decays, where charged particles are misidentified and neutrals are missing, namely:  $D^+ \rightarrow K^-\pi^+\pi^+$ ,  $D_s^+ \rightarrow K^-K^+\pi^+$ ,  $D^+ \rightarrow K^-K^+\pi^+$ ,  $D^+ \rightarrow \pi^+\pi^-\pi^+$ ,  $D^+ \rightarrow K^-\pi^+\mu^+\nu$ ,  $D_s^+ \rightarrow K^-K^+\mu^+\nu$  and  $D^+ \rightarrow K^-\pi^+\pi^+\pi^0$ . For each of them we evaluate the number and the distribution shape of events which survive the selection cuts and penetrate into the  $D^+$  and  $D_s^+ \rightarrow K^+\pi^+\pi^-$  signal and sideband regions. From this study, we find that the major contributions for  $D^+$  come from  $D^+ \rightarrow K^-\pi^+\pi^+$ ,  $D_s^+ \rightarrow K^-K^+\pi^+$  and  $D^+ \rightarrow K^-\pi^+\pi^+\pi^0$ , and for  $D_s^+$  from  $D^+ \rightarrow K^-\pi^+\pi^+$ ,  $D^+ \rightarrow \pi^+\pi^-\pi^+$  and  $D^+ \rightarrow K^-\pi^+\pi^+\pi^0$ . In Fig. 1 the selected  $K^+\pi^+\pi^-$  combinations for  $D^+$  and  $D_s^+$  are shown, along with the distribution of the Monte Carlo reflected events. We choose to start our fit from the  $1.75 \text{ GeV}/c^2$  energy threshold since the region below is dominated by the partial reconstruction of multi-body charm channels where neutrals are missing. The signal yields consist of  $189 \pm 24$  events for  $D^+$  and  $567 \pm 31$  events for  $D_s^+$ . The fits are performed with two Gaussian functions for the signals and a second order

---

<sup>1</sup> The sidebands for  $D^+$  cover the  $-5\sigma$  to  $-3\sigma$  and the  $3\sigma$  to  $5\sigma$  regions from the  $D^+$  peak. For the  $D_s^+$  the left sideband covers the  $-5\sigma$  to  $-3\sigma$  region and the right sideband covers the  $4\sigma$  to  $6\sigma$  region, both from the  $D_s^+$  peak.

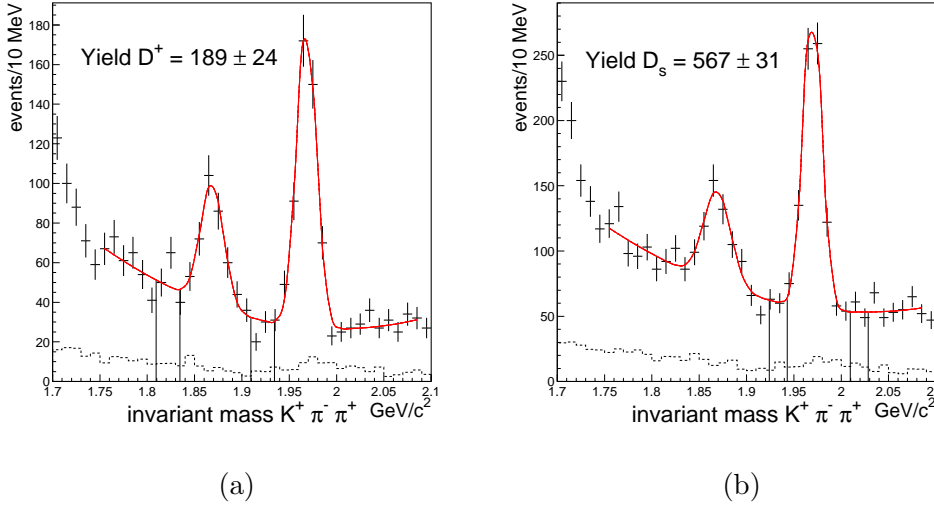


Figure 1. Invariant mass distributions  $K^+\pi^+\pi^-$  with final selection criteria for (a)  $D^+$  and (b)  $D_s^+$ , along with distributions of the residual reflected events expected from Monte Carlo (dotted curves). In the picture the sideband regions (vertical lines) are also shown.

polynomial for the background. Centroid and width are  $1.869 \pm 0.002$   $\text{GeV}/c^2$  and  $0.012 \pm 0.002$   $\text{GeV}/c^2$  for  $D^+$  (Fig. 1(a)), and  $1.970 \pm 0.001$   $\text{GeV}/c^2$  and  $0.010 \pm 0.001$   $\text{GeV}/c^2$  for  $D_s^+$  (Fig. 1(b)). The measured widths are in good agreement with the Monte Carlo predictions. The signal to noise ratio are  $1.0 \pm 0.1$  and  $2.4 \pm 0.4$  for  $D^+$  and  $D_s^+$ , respectively. The reflected events are smoothly distributed across the invariant mass spectrum and are thus properly accounted for by the background polynomial fitting function.

Residual structures induced by reflections in the Dalitz plot signal and sideband regions are a potential source of systematics of our amplitude analysis. The shape of the background in the Dalitz signal region is parametrized through a fit to the Dalitz plot of mass sidebands, which consists of a polynomial plus Breit-Wigner functions to account for any feed-through from resonances. We verify that the reflections in the sidebands are well described by this simple background fit function and adequately represent the reflections in the signal regions.

### 3 Branching ratio results

The DCS  $D^+ \rightarrow K^+\pi^+\pi^-$  decay fraction is evaluated with respect to the CF  $D^+ \rightarrow K^-\pi^+\pi^+$  mode, the SCS  $D_s^+ \rightarrow K^+\pi^+\pi^-$  with respect to the CF  $D_s^+ \rightarrow K^-K^+\pi^+$  mode. In Fig. 2 the mass distributions for the normalization

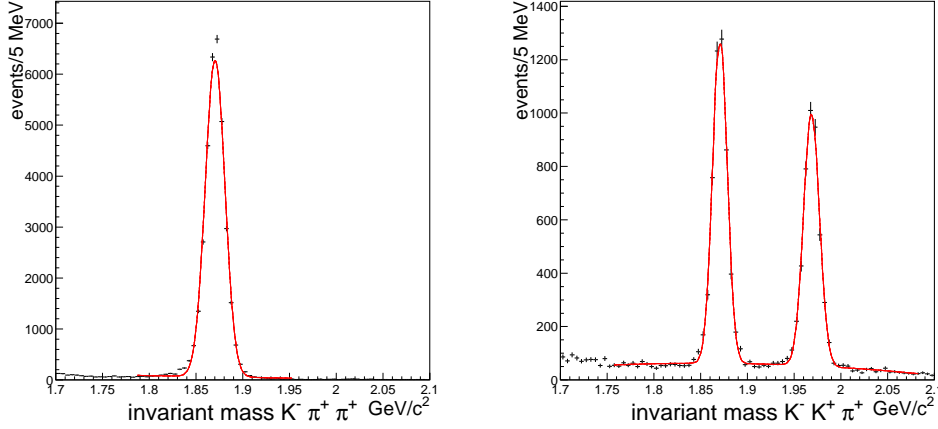


Figure 2. Invariant mass distributions of  $D^+ \rightarrow K^- \pi^+ \pi^+$  and  $D_s^+ \rightarrow K^- K^+ \pi^+$  normalization channels.

channels are shown. The CF  $D^+ \rightarrow K^- \pi^+ \pi^+$  sample is selected with the same set of cuts as for the DCS channel, in order to minimize systematic effects; the signal yield is  $32714 \pm 184$ . The CF  $D_s^+ \rightarrow K^- K^+ \pi^+$  is obtained requiring for  $K^-$  a  $\Delta W_K > 2$  similar to the  $\Delta W_\pi$  for the opposite-sign pion in the SCS selection; kinematical cuts are applied to remove the reflections in the  $K^- K^+ \pi^+$  mode from the CF  $D^+ \rightarrow K^- \pi^+ \pi^+$  and from  $D^{*+} \rightarrow D^0 \pi^+$ , followed by the  $D^0$  decay to  $K^- \pi^+$ . The  $D_s^+ \rightarrow K^- K^+ \pi^+$  signal yield is  $4033 \pm 68$ . A fully coherent generation is used both for the channels under study and the normalization modes; the relative efficiencies are measured to be

$$\frac{\epsilon(D^+ \rightarrow K^+ \pi^+ \pi^-)}{\epsilon(D^+ \rightarrow K^- \pi^+ \pi^+)} = 0.888 \pm 0.006 \quad (1)$$

and

$$\frac{\epsilon(D_s^+ \rightarrow K^+ \pi^+ \pi^-)}{\epsilon(D_s^+ \rightarrow K^- K^+ \pi^+)} = 1.106 \pm 0.009. \quad (2)$$

From the yields and efficiency ratios, we measure the following branching ratios,

$$\frac{\Gamma(D^+ \rightarrow K^+ \pi^+ \pi^-)}{\Gamma(D^+ \rightarrow K^- \pi^+ \pi^+)} = 0.0065 \pm 0.0008 \pm 0.0004 \quad (3)$$

and

$$\frac{\Gamma(D_s^+ \rightarrow K^+ \pi^+ \pi^-)}{\Gamma(D_s^+ \rightarrow K^- K^+ \pi^+)} = 0.127 \pm 0.007 \pm 0.014. \quad (4)$$

The first error reported is statistical and the second is systematic.

To evaluate the systematic error we consider, as done in other FOCUS analyses [5, 6], three contributions, which are added in quadrature to obtain the global systematic error: the *split sample*, *fit variant* and *cut variant* components. The *split sample* component takes into account the systematics intro-

duced by residual difference between data and Monte Carlo, due to a possible mismatch in the reproduction of the  $D$  momentum and the changing experimental conditions of the spectrometer during data collection. This component has been determined by splitting data into four independent subsamples, according to the  $D$  momentum range (high and low momentum) and the configuration of the vertex detector. The *S-factor method* from the Particle Data Group [7] was used to try to separate true systematic variations from statistical fluctuations. The branching ratio is evaluated for each of the four statistically independent subsamples and a *scaled variance* is calculated  $\tilde{\sigma}$  (the errors are boosted when  $\chi^2/(N-1) > 1$ ). The *split sample* variance is defined as the difference between the reported statistical variance and the scaled variance, if the scaled variance exceeds the statistical variance. Another possible source of systematics uncertainty is the *fit variant*. This component is computed by varying the fitting conditions on the whole data set. In our study fit variants include the background and signal shape, the bin size of the mass-distribution histogram and the Monte Carlo generation modeling. More precisely different degrees of the polynomial functions are used for the background parametrization and two Gaussian peaks with the same mean but different widths are used for the signal, to take into account the different resolution in momentum of our spectrometer. The fully coherent generation for the decays under analysis is based on the results of the Dalitz plot study presented in this paper (see paragraph 4.3). To access a possible systematics effect in the branching ratio evaluation coming from our amplitude analysis we vary coefficients and phases returned by the Dalitz plot fit within their errors. The branching ratio values obtained by these variants are all a priori likely, therefore this uncertainty can be estimated by the standard deviation of the measurements. To investigate the dependence of the branching ratio on the particular choice of cuts we calculate a *cut variant* error, analogously to the *fit variant*, by using the standard deviation of different branching ratio measurements obtained with several sets of cuts; this error is actually overestimated since the statistics of the cut samples are different.

For the  $D^+$  the dominant systematic effect comes from the *cut variant*, while for the  $D_s^+$  the main source of uncertainty comes from the *split sample* component. Our results are consistent with previous determinations from the E687 [8] and E791 [9] experiments. Our measurements reduce the statistical errors by about a factor of 2 and 5 for the  $D^+$  and  $D_s^+$ , respectively.

## 4 Dalitz plot analysis

Events within  $\pm 2\sigma$  of the mass peak are used to perform the Dalitz plot analysis for  $D^+$  and  $D_s^+ \rightarrow K^+\pi^+\pi^-$ ; the  $D^+$  and  $D_s^+$  Dalitz plots are shown in Fig.3 a) and b), respectively.

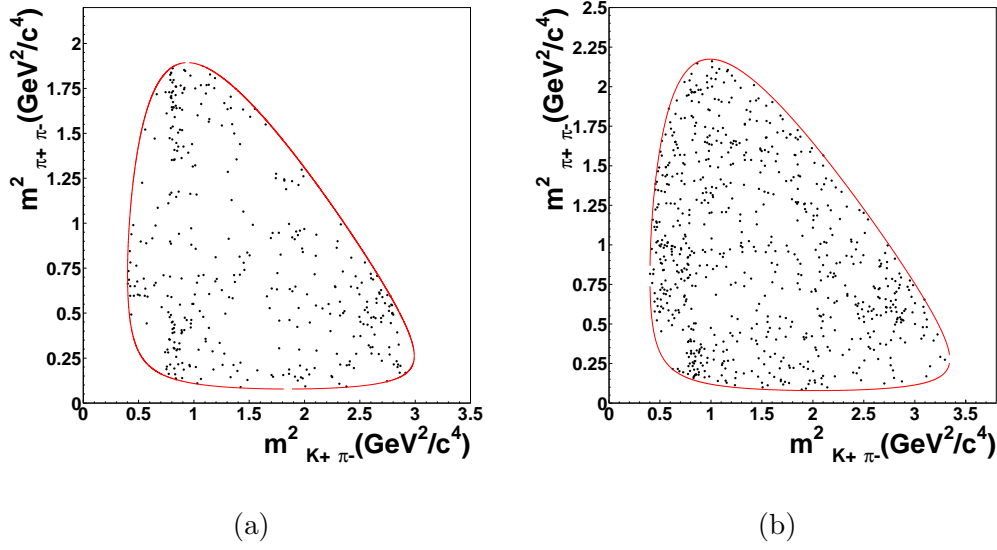


Figure 3. a)  $D^+$  and b)  $D_s^+$  Dalitz plots in  $K^+\pi^-$  and  $\pi^+\pi^-$  squared mass contributions.

#### 4.1 The decay amplitude

For this analysis we use a formalization of the decay amplitude based on the simple isobar model, which is viewed as an effective description of the main dynamical features of the decay. More rigorous treatments, such as that based on the  $K$ -matrix formalism [10], are not viable for this analysis because of the limited statistics of the samples, along with the large number of free parameters necessary to account for the simultaneous presence of both  $\pi^+\pi^-$  and  $K^+\pi^-$  resonances.

The decay matrix element for the analysis reported here is written as a coherent sum of amplitudes corresponding to a constant term for the uniform direct three-body decay and to different resonant channels:

$$\mathcal{M} = a_0 e^{i\delta_0} + \sum_j a_j e^{i\delta_j} B(abc|r) \quad (5)$$

where  $a, b$  and  $c$  label the final-state particles.  $B(abc|r) = B(a, b|r)S(a, c)$  where  $B(a, b|r)$  is the Breit-Wigner function

$$B(a, b|r) = \frac{F_D F_r}{M_r^2 - M_{ab}^2 - i\Gamma M_r} \quad (6)$$

and  $S(a, c) = 1$  for a spin-0 resonance,  $S(a, c) = -2\mathbf{c} \cdot \mathbf{a}$  for a spin-1 resonance and  $S(a, c) = 2(|\mathbf{c}||\mathbf{a}|)^2(3\cos^2\theta^* - 1)$  for a spin-2 state.  $\mathbf{a}$  and  $\mathbf{c}$  are the three-



momenta of particles  $a$  and  $c$  measured in the  $ab$  rest frame, and  $\cos\theta^* = \mathbf{c} \cdot \mathbf{a}/|\mathbf{c}||\mathbf{a}|$ . The momentum-dependent form factors  $F_D$  and  $F_r$  represent the strong coupling at each decay vertex. For each resonance of mass  $M_r$  and spin  $j$  we use a width

$$\Gamma = \Gamma_r \left( \frac{p}{p_r} \right)^{2j+1} \frac{M_r}{M_{ab}} \frac{F_r^2(p)}{F_r^2(p_r)} \quad (7)$$

where  $p$  is the decay three-momentum in the resonance rest frame and the subscript  $r$  denotes the on-shell values. The order of the particle labels is important for defining the phase convention; here the first particle is the opposite-sign one.

For the  $f_0(980)$  a simple single-channel Breit-Wigner is used. The mass and width values of  $0.972 \pm 0.002$  GeV and  $0.059 \pm 0.004$  GeV, respectively, are obtained from a fit to our FOCUS Dalitz plot of the  $D_s^+ \rightarrow \pi^+\pi^-\pi^+$  channel, where the  $f_0(980)$  is the dominant component. Given the questionable assumption of a single channel Breit-Wigner, where a coupled-channel one should be more properly used, we have checked that the final results do not change when a Flatté parametrization [11] is used.

#### 4.2 The likelihood function and fitting procedure

Following our previous analyses [10, 12, 13] we perform a maximum likelihood fit to the Dalitz plots to measure the coefficients of the various decay amplitudes as well as their relative phases. The probability density function is corrected for geometrical acceptance and reconstruction efficiency. The shape of the background in the signal region is parametrized through an incoherent sum of a polynomial function plus resonant Breit-Wigner components, which are used to fit the Dalitz plot of mass sidebands. The number of background events expected in the signal region is estimated through fits to the  $K^+\pi^+\pi^-$  mass spectrum. All background parameters are included as additional fit parameters and tied to the results of the sideband fits through the inclusion in the likelihood of a  $\chi^2$  penalty term derived from the covariance matrix of the sideband fit. The  $D^+$  and  $D_s^+$  samples are fitted with likelihood functions  $\mathcal{L}$  consisting of signal and background probability densities. Checks for fitting procedure are made using Monte Carlo techniques and all biases are found to be small compared to the statistical errors. The systematic errors on our results are evaluated following the strategy already explained for the branching ratio measurements, defining a *split-sample* and a *fit-variant* component. The assumption that the shape of the background in the sideband is a good representation of the background in the signal region potentially constitutes a source

of systematic error. We take into account this effect in the *fit-variant* error, by varying the polynomial function degree and adding/removing the Breit-Wigner terms, which are introduced to take into account any feed-through from resonances in the background, and computing the standard deviation of the different results.

In our Dalitz plot analysis we allow for the possibility of contributions from all known  $K^+\pi^-$  and  $\pi^+\pi^-$  resonances [7] and from a flat non-resonant contribution accounting for the direct decay of the D mesons into three-body final states. The fit parameters are amplitude coefficients  $a_j$  and phases  $\delta_j$ .<sup>2</sup> The general procedure, adopted for all the fits reported here, consists of several successive steps in order to eliminate contributions whose effects on our fit are marginal. Contributions are removed if their amplitude coefficients,  $a_0$  and  $a_i$  of Eq. 5 are less than  $3\sigma$  significant *and* the fit confidence level increases due to the decreased number of degrees of freedom in the fit. The fit confidence levels (C.L.) are evaluated with a  $\chi^2$  estimator over a Dalitz plot with bin size adaptively chosen to maintain a minimum number of events in each bin. Once the minimal set of parameters is determined, addition of each single contribution previously eliminated is reinstated to verify if the C.L. improves; in this case the contribution is added in the final set.

### 4.3 Results

The  $D^+$  and  $D_s^+$  Dalitz plots present a different event intensity distribution. The  $D^+$  appears highly structured and dominated by  $\rho(770)$  and  $K^*(892)$ . The  $D_s^+$  channel, instead, presents a much more complex structure diffused over all the phase-space together with  $\rho(770)$  and  $K^*(892)$ , whose main characteristics are still visible. These general features are confirmed by our fits.

In Table 1, fit fractions,<sup>3</sup> phases and coefficients of the various amplitudes describing the  $D^+ \rightarrow K^+\pi^+\pi^-$  decay are reported. The vector resonances  $\rho(770)$  and  $K^*(892)$  account for about 90% of the  $D^+$  decay fraction. Their relative phase difference, almost real, suggests a marginal role for final state interactions in this decay. The C.L. of our Dalitz plot fit is 9.2%. The three-lobe helicity structure visible in the  $D^+$  Dalitz plot justifies the presence of the tensor  $K_2^*(1430)$ , at more than three sigma statistical significance, in the final set of resonances. The band of events at about  $(1 \text{ GeV}/c^2)^2$  in the  $m_{\pi^+\pi^-}^2$  mass combination indicates the presence of the scalar  $f_0(980)$  in the decay at a

<sup>2</sup> Coefficients and phases of the  $\rho(770)$ , which is a dominant mode in both decays, are fixed to 1 and 0, respectively.

<sup>3</sup> The quoted fit fractions are defined as the ratio between the intensity for a single amplitude integrated over the Dalitz plot and that of the total amplitude with all the modes and interferences present.

Decay channel	Fit fraction (%)	Phase $\phi_j$ (degrees)	Amplitude coefficient
$\rho(770)K^+$	$39.43 \pm 7.87 \pm 8.15$	0 (fixed)	1 (fixed)
$K^*(892)\pi^+$	$52.20 \pm 6.84 \pm 6.38$	$-167.1 \pm 14.4 \pm 23.0$	$1.151 \pm 0.173 \pm 0.161$
$f_0(980)K^+$	$8.92 \pm 3.33 \pm 4.12$	$-134.5 \pm 31.4 \pm 41.9$	$0.476 \pm 0.111 \pm 0.143$
$K_2^*(1430)\pi^+$	$8.03 \pm 3.72 \pm 3.91$	$54.4 \pm 38.3 \pm 20.9$	$0.451 \pm 0.125 \pm 0.129$
C.L. = 9.2%	$\chi^2 = 13.6$	d.o.f. = 21 (#bins) - 13 (#free parameters)	

Table 1

Dalitz plot fit results for the  $D^+ \rightarrow K^+\pi^+\pi^-$  final state.

four sigma significance level. The absence in the  $K^+\pi^-$  combination of scalar  $K_0^*(1430)$ , while the tensor  $K_2^*(1430)$  is present, seems to us a bit suspicious; further investigations would required higher statistics. It is nevertheless interesting to observe that the DCS decay  $D^+ \rightarrow K^+\pi^+\pi^-$  is dominated by vector resonances with no major role of rescattering effects. The results of the fit on the two invariant mass squared projections  $m_{K\pi}^2$  and  $m_{\pi\pi}^2$  are shown in Fig. 4.

An amplitude analysis of this decay has been previously performed by the E791 experiment [9], which described the decay with two resonant channels,  $\rho(770)K^+$  and  $K^*(892)\pi^+$ , plus a uniform non-resonant component, each accounting for about 1/3 of the decay fraction; the non-resonant contribution seems to be better resolved in the present analysis in additional resonant channels. We observe that the E791  $\rho(770)/K^*(892)$  relative phase difference<sup>4</sup> is about  $0^\circ$  while our measurement is close to  $180^\circ$ . We also perform a fit of our sample with the same components as E791. The results still confirm the disagreement.

In Table 2, the fit fractions, phases and coefficients resulting from the  $D_s^+$  fit are reported. As for the  $D^+$ , the  $\rho(770)$  and  $K^*(892)$  vector resonances represent the major contributions and cover about 60% of the decay fraction; their phase shift configuration is almost real for this decay as well. The description of the event intensity all over the Dalitz plot requires three higher mass resonances, two in  $K^+\pi^-$  and one in  $\pi^+\pi^-$ , and a non-resonant term. More precisely the two  $K^+\pi^-$  states are the scalar  $K_0^*(1430)$  and the vector  $K^*(1410)$ , which are the lowest mass resonances besides the  $K^*(892)$ , and the  $\pi^+\pi^-$  state is  $\rho(1450)$ , which is the second vector state in the  $\rho$  series. They account for an additional 30–40% resonant portion of the decay; a non-resonant contribution of about 15% completes the event description for this channel. The fit C.L. for the mixture of states selected is 5.5%.

This solution satisfactory reproduces the main features of the decay, as indicated by the C.L., and shown in the two invariant mass squared projections

<sup>4</sup> This relative phase difference is free of phase convention ambiguity.

Decay channel	Fit fraction (%)	Phase $\phi_j$ (degrees)	Amplitude coefficient
$\rho(770)K^+$	$38.83 \pm 5.31 \pm 2.61$	0 (fixed)	1 (fixed)
$K^*(892)\pi^+$	$21.64 \pm 3.21 \pm 1.14$	$161.7 \pm 8.6 \pm 2.2$	$0.747 \pm 0.080 \pm 0.031$
$NR$	$15.88 \pm 4.92 \pm 1.53$	$43.1 \pm 10.4 \pm 4.4$	$0.640 \pm 0.118 \pm 0.026$
$K^*(1410)\pi^+$	$18.82 \pm 4.03 \pm 1.22$	$-34.8 \pm 12.1 \pm 4.3$	$0.696 \pm 0.097 \pm 0.025$
$K_0^*(1430)\pi^+$	$7.65 \pm 5.0 \pm 1.70$	$59.3 \pm 19.5 \pm 13.2$	$0.444 \pm 0.141 \pm 0.060$
$\rho(1450)K^+$	$10.62 \pm 3.51 \pm 1.04$	$-151.7 \pm 11.1 \pm 4.4$	$0.523 \pm 0.091 \pm 0.020$
C.L. = 5.5%	$\chi^2 = 38.5$	d.o.f. = 43 (#bins) - 17 (#free parameters)	

Table 2

Dalitz plot fit results for the  $D_s^+ \rightarrow K^+\pi^+\pi^-$  final state.

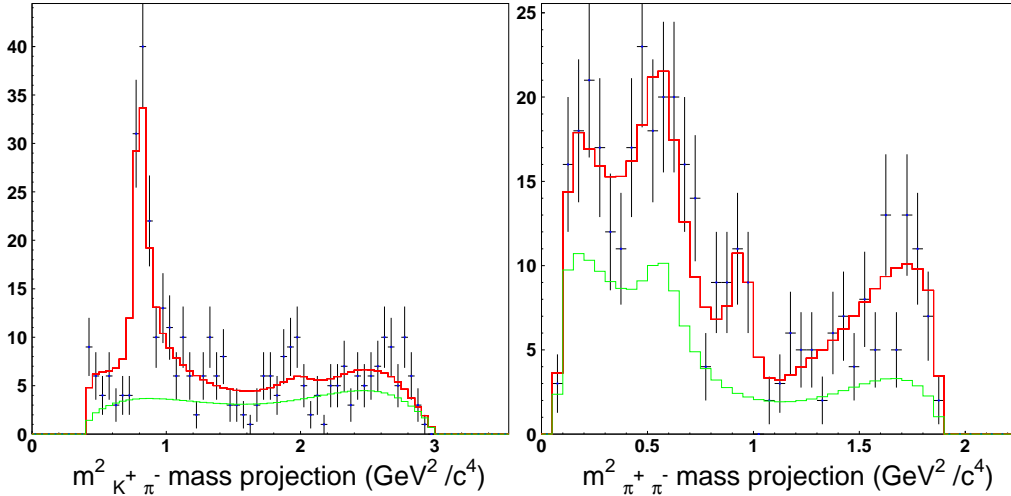


Figure 4. The Dalitz plot projections and, superimposed, the fit results for  $D^+$ . The background shape under the signal is also shown.

$m_{K\pi}^2$  and  $m_{\pi\pi}^2$  of the Dalitz plot in Fig. 5. However the absence of the  $f_0(980)$  in the fit is a bit suspicious; an accumulation of events at  $(1 \text{ GeV}/c^2)^2$   $\pi^+\pi^-$  mass squared, to some extent visually recognizable in the Dalitz plot, would indeed suggest its selection in the resonance final set. On the other hand we know that the isobar model is too naive to describe more complex decays dynamics, which intervenes in the presence of the  $K^+\pi^-$  and  $\pi^+\pi^-$  S-waves states. More rigorous treatments, such as that based on the  $K$ -matrix model [10], will be necessary at higher statistics. The results of the fit on the squared invariant masses  $m_{K\pi}^2$  and  $m_{\pi\pi}^2$  are shown in Fig. 5.

The dominant systematic uncertainties on coefficients and phases for both  $D^+$  and  $D_s^+$  decays come from the low/high momentum split and the fit variant component.

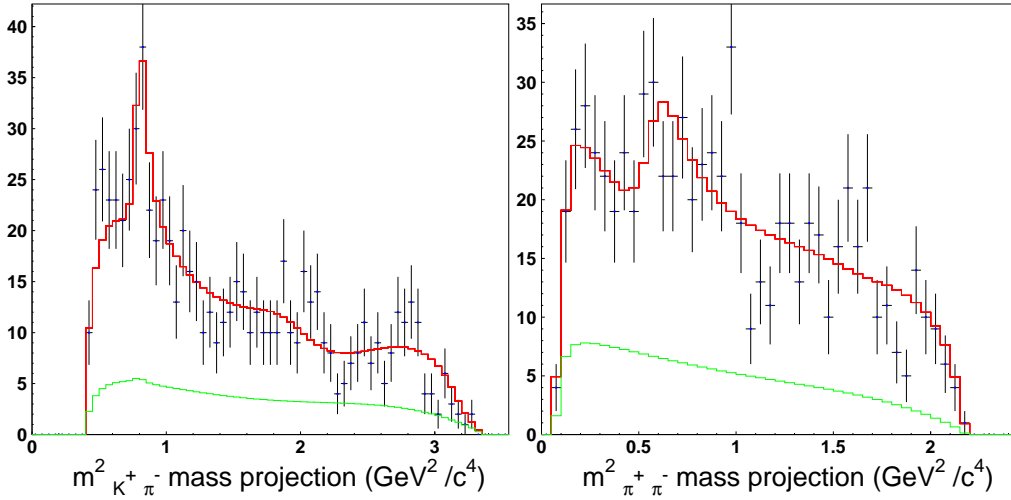


Figure 5. The Dalitz plot projections and, superimposed, the fit results for  $D_s^+$ . The background shape under the signal is also shown.

## 5 Conclusions

We have presented a study of the doubly and singly Cabibbo suppressed decays  $D^+$  and  $D_s^+ \rightarrow K^+\pi^+\pi^-$ . Our measurements of  $\Gamma(D^+ \rightarrow K^+\pi^+\pi^-)/\Gamma(D^+ \rightarrow K^-\pi^+\pi^+) = 0.0065 \pm 0.0008 \pm 0.0004$  and  $\Gamma(D_s^+ \rightarrow K^+\pi^+\pi^-)/\Gamma(D_s^+ \rightarrow K^+K^-\pi^+) = 0.127 \pm 0.007 \pm 0.014$  improve the statistical accuracy by approximately a factor of 2 and 5 with respect to previous determinations. In particular the comparison of  $(1/\tan^4\theta_C) \times \Gamma(D_{\text{DCS}}^+)/\Gamma(D_{\text{CF}}^+) = 2.60 \pm 0.32$  with the FOCUS lifetime ratio of  $\tau(D^+)/\tau(D^0) = 2.538 \pm 0.023$  and the marginal role of FSI inferred by our Dalitz plot analysis of this decay supports the interpretation that destructive interference between spectator amplitudes with indistinguishable quarks in the CF  $D^+$  final state is responsible for the lifetime difference between  $D^+$  and  $D^0$ . The FOCUS collaboration has already analysed the doubly Cabibbo suppressed decay of the neutral meson  $D^0 \rightarrow K^+\pi^-$  [14]; the study of the DCS decay of the charged  $D^+$  meson presented in this paper, free of any possible uncertainty due to  $D^0\bar{D}^0$  mixing effects, provides complementary information. The amplitude analysis of  $D^+$  and  $D_s^+ \rightarrow K^+\pi^+\pi^-$  final states have also been performed, providing the first amplitudes and phases for the  $D_s^+$  channel. We have discussed the major achievements and indicated possible improvements for a better decay dynamics interpretation at higher statistics.

We wish to acknowledge the assistance of the staffs of Fermi National Accelerator Laboratory, the INFN of Italy, and the physics departments of the collaborating institutions. This research was supported in part by the US National Science Foundation, the US Department of Energy, the Italian Istituto Nazionale di Fisica Nucleare and Ministero dell'Istruzione dell'Università e

della Ricerca, the Brazilian Conselho Nacional de Desenvolvimento Científico e Tecnológico, CONACyT-México, the Korean Ministry of Education, and the Korean Science and Engineering Foundation.

## References

- [1] J. M. Link *et al.*, Phys. Lett. B **537** (2002) 192.
- [2] P. L. Frabetti *et al.* Nucl. Instrum. Meth. A **320** (1992) 519.
- [3] J. M. Link *et al.*, Nucl. Instrum. Meth. A **484** (2002) 270.
- [4] J. M. Link *et al.*, Phys. Lett. B **485** (2000) 62.
- [5] J. M. Link *et al.*, Phys. Lett. B **555** (2003) 167.
- [6] J. M. Link *et al.*, Phys. Lett. B **575** (2003) 190.
- [7] K. Hagiwara *et al.* (Particle Data Group), Phys. Rev. D **66** (2002) 010001.
- [8] P. L. Frabetti *et al.*, Phys. Lett. B **359** (1995) 403.
- [9] E. M. Aitala *et al.*, Phys. Lett. B **404** (1997) 187.
- [10] J. M. Link *et al.*, Phys. Lett. B **585** (2004) 200.
- [11] S. M. Flatte, Phys. Lett. B **63** (1976) 228.
- [12] P. L. Frabetti *et al.*, Phys. Lett. B **407** (1997) 79.
- [13] P. L. Frabetti *et al.*, Phys. Lett. B **351** (1995) 591.
- [14] J. M. Link *et al.*, Phys. Rev. Lett. **86** (2001) 2955.